



## **STRAIN LIMITS AND PLASTIC HINGE LENGTHS FOR DISPLACEMENT BASED SEISMIC DESIGN OF CIRCULAR BRIDGE COLUMNS**

J. C. Goodnight<sup>(1)</sup>, M. J. Kowalsky<sup>(2)</sup>, J. M. Nau<sup>(3)</sup>

<sup>(1)</sup> *Engineer, WSP, chad.goodnight@wsp.com (Former Postdoc at North Carolina State University)*

<sup>(2)</sup> *Professor, North Carolina State University, kowalsky@ncsu.edu*

<sup>(3)</sup> *Professor, North Carolina State University, nau@ncsu.edu*

### ***Abstract***

This paper discusses performance strain limit and plastic hinge length recommendations for displacement-based seismic design of circular reinforced concrete bridge columns. These recommendations were obtained via analysis of results from thirty unidirectional and twelve bidirectional experiments that contained instrumentation capable of measuring distributions of strain and curvature along the member length. The main experimental variables included longitudinal and transverse steel content, axial load ratio, aspect ratio, and lateral displacement history. Expressions that predict concrete and steel strains preceding important limit states were created, which included: cover concrete crushing, initial yielding of confinement steel, and longitudinal bar buckling. Since bar buckling, and subsequent fracture, limited the deformation capacity of the well-confined columns, separate expressions that provided either a mean value prediction or a reduced probability of bar buckling were produced. A modified plastic hinge method was created to convert curvatures at limit state strains to lateral displacements. Separate tensile and compressive plastic hinge lengths were recommended for respective conversions of material strain to displacement. The tensile plastic hinge length was formulated to match the measured extent of plasticity, which also provided accurate tensile strain-displacement relationships necessary for bar buckling predictions. The compressive plastic hinge length matches current AASHTO Guide Specifications for LRFD Seismic Bridge Design recommendations, which reference Priestley et al. (1996). The compressive plastic hinge length is recommended for both compressive strain-displacement and for predictions of member force versus deformation, thus nonlinear static pushover procedures remain unchanged and the tensile hinge length is exclusively used to convert plastic curvatures at tensile strain limits to lateral displacements. The modified plastic hinge method and performance strain limit recommendations discussed herein can be used to define the target displacement for input into Direct Displacement-Based Design or to evaluate the displacement capacity following nonlinear static pushover procedures outlined in the AASHTO Guide Specifications for LRFD Seismic Bridge Design.

*Keywords: displacement-based design; bridge column; plastic hinge length; strain limits; longitudinal bar buckling*

## 1. Introduction

This paper discusses performance strain limit and plastic hinge length recommendations for displacement-based seismic design of circular reinforced concrete bridge columns. These recommendations were obtained via analysis of results from thirty unidirectional [1] and twelve bidirectional [2] experiments that contained instrumentation capable of measuring distributions of strain and curvature along the member length. The main experimental variables included longitudinal and transverse steel content, axial load ratio, aspect ratio, and lateral displacement history. Design recommendations discussed herein replace those in [3&4] and include data from the more recent bidirectional dataset in Table 1. An overview of the specimen geometry, test setup, and typical bidirectional load path appears in Figs. 1 and 2. Lateral actuators applied quasi-static loading to the top of the cantilever columns. A constant axial load was applied using an internal unbonded post-tensioning bar. Additional details regarding the experimental programs appear in [1&2]. Here, sample test results are provided to describe the typical progression of damage and the process for obtaining measured strain and curvature data used to generate the performance strain limits and plastic hinge length recommendations.

Expressions that predict concrete and steel strains preceding important limit states were created, which included: cover concrete crushing, initial yielding of confinement steel, and longitudinal bar buckling. Since bar buckling, and subsequent fracture, limited the deformation capacity of the well-confined columns, separate expressions that provided either a mean value prediction or a reduced probability of bar buckling were produced. A modified plastic hinge method was created to convert curvatures at limit state strains to lateral displacements. Separate tensile and compressive plastic hinge lengths were recommended for respective conversions of material strain to displacement. The tensile plastic hinge length was formulated to match the measured extent of plasticity, which also provided accurate tensile strain-displacement relationships necessary for bar buckling predictions. The compressive plastic hinge length matches current Seismic Guide Specifications [5] recommendations, which reference [6]. The compressive plastic hinge length is used for both compressive strain-displacement and for predictions of member force versus deformation, thus nonlinear static pushover procedures remain unchanged and the tensile hinge length is exclusively used to convert plastic curvatures at tensile strain limits to lateral displacements. A second nonlinear static pushover is not required.

The modified plastic hinge method and performance strain limits discussed herein can be used to define the target displacement for input into Direct Displacement-Based Design [7] or to evaluate the displacement capacity following nonlinear static pushover procedures outlined in the Seismic Guide Specifications [5].

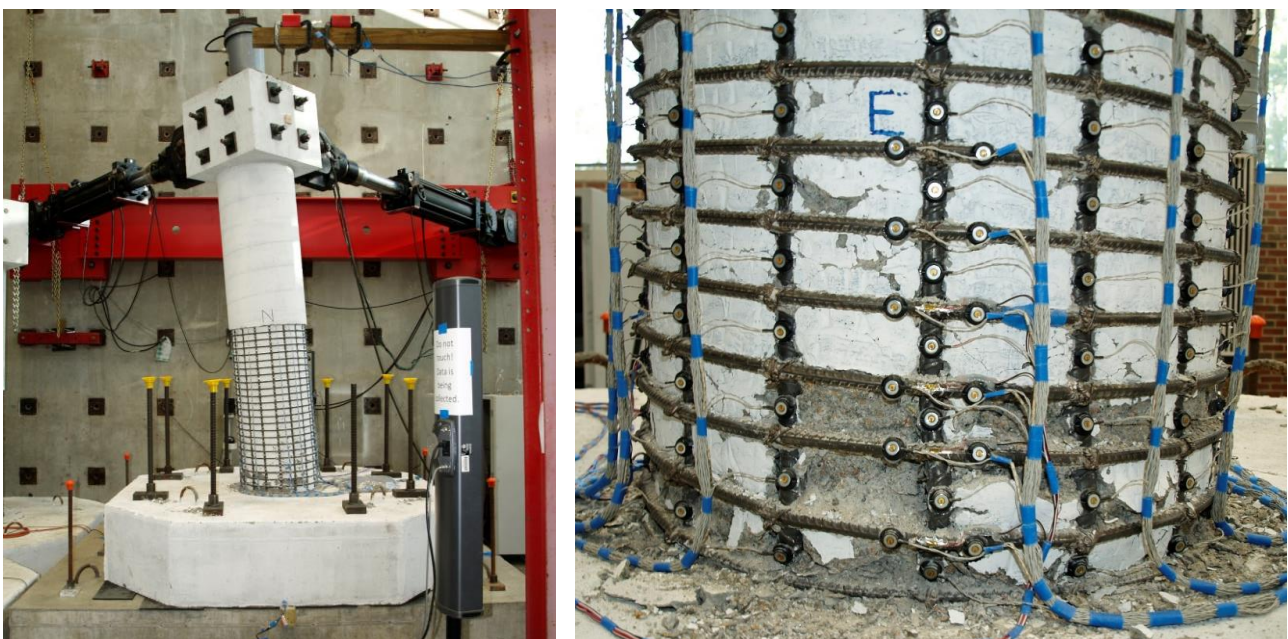


**Fig. 1** – Deformed Specimen #11 at  $\mu_{\Delta 7}^{+1x} = 8.49''$  with Multiple Buckled East Longitudinal Bars

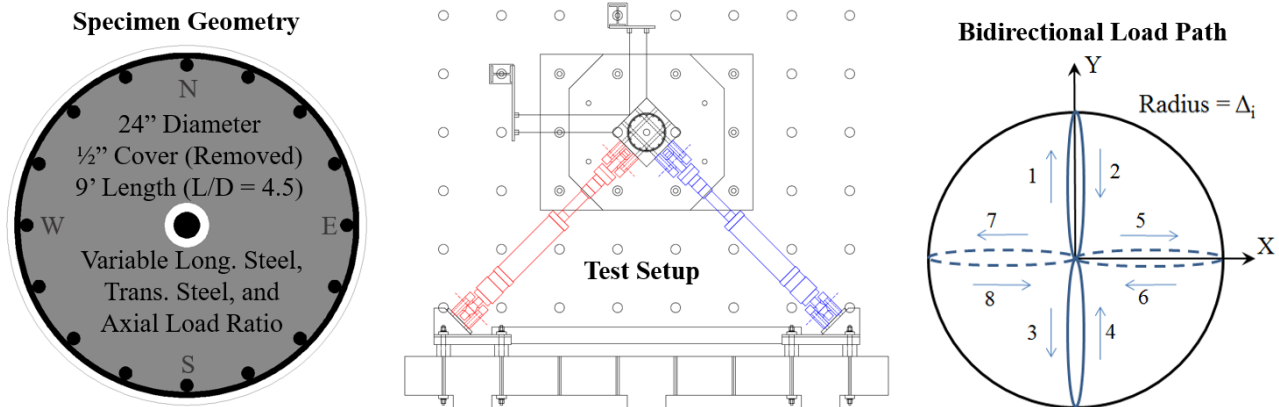


Fig. 2 – Specimen Geometry, Test Setup, and Bidirectional Load Path

Table 1 – Test Matrix for the Bidirectional Dataset

Test	Load Path	Longitudinal	Ast/Ag	Transverse	4Asp/D's	P/f'cAg
1	2-Cycle-Set	16 #7	0.021	#3 at 2.75"	0.007	0.074
2	3-Cycle-Set	16 #7	0.021	#3 at 2.75"	0.007	0.075
3	Asymmetric 2-Cycle-Set	16 #7	0.021	#3 at 2.75"	0.007	0.074
4	2-Cycle-Set	16 #7	0.021	#3 at 2"	0.01	0.06
5	3-Cycle-Set	16 #7	0.021	#3 at 2"	0.01	0.06
6	Asymmetric 2-Cycle-Set	16 #7	0.021	#3 at 2"	0.01	0.059
7	2-Cycle-Set	16 #6	0.016	#3 at 1.5"	0.013	0.079
8	2-Cycle-Set	16 #6	0.016	#3 at 2"	0.01	0.074
9	2-Cycle-Set	16 #6	0.016	#3 at 2.75"	0.007	0.073
10	2-Cycle-Set	16 #7	0.021	#3 at 1.5"	0.013	0.075
11	Megathrust	16 #6	0.016	#3 at 2"	0.01	0.075
12	Megathrust	16 #6	0.016	#3 at 2.75"	0.007	0.074

## 2. Sample Test Results for Specimen #11 – Bidirectional Megathrust Loading

In this section, sample test results for Specimen #11 are provided to describe the typical progression of damage and the process for obtaining measured strain and curvature data used to generate the performance strain limits and plastic hinge length recommendations. Test #11 had a 24" diameter circular cross section, an aspect ratio of 4.5, a longitudinal steel content of 1.6%, a transverse volumetric steel ratio of 1%, and an axial load ratio of 7.5%. A bidirectional adaptation of the subduction event megathrust load history recommended in [8] was selected for Test #11. A full test summary including material properties, observed damage, and analysis of the measured data appears in [2]. The megathrust load history and resulting hysteretic response is shown in Figs. 3 and 4 with data labels that note key damage observations. A peak displacement ductility demand of seven was selected based on the deformation capacity of a nominally identical specimen subjected to a more typical symmetric two-cycle-set load protocol. In comparison, the megathrust load history had additional low ductility cycles, but comparatively fewer high ductility cycles when scaled the same peak displacement.

The following progression of damage was observed in each experiment: cracking, initial yielding of longitudinal steel, cover concrete crushing, yielding of confinement steel, buckling of longitudinal reinforcement, core concrete damage behind buckled reinforcement, and fracture of previously buckled bars or confining steel. Specimen #11 was saved for repair following the first bar fracture, but results of prior specimens highlight that fracture of previously buckled reinforcement represents the first significant loss in strength for well-confined bridge columns. In Test #11, initial buckling of longitudinal reinforcement was observed during the peak cycle at displacement ductility seven, while a single post-peak cycle at displacement ductility 4.5 was sufficient to fracture previously buckled reinforcement. A photo of buckled east

reinforcement at the peak displacement appears in Fig. 1. Note that bar buckling is a behavior that occurs over multiple layers of transverse steel in well-confined columns. Fracture of previously buckled reinforcement is related to exceedance of a critical bending strain in regions of increased buckling induced deformation. This highlights the importance of identifying initial bar buckling as a key performance limit state for bridge columns, since it ultimately precipitates bar fracture.

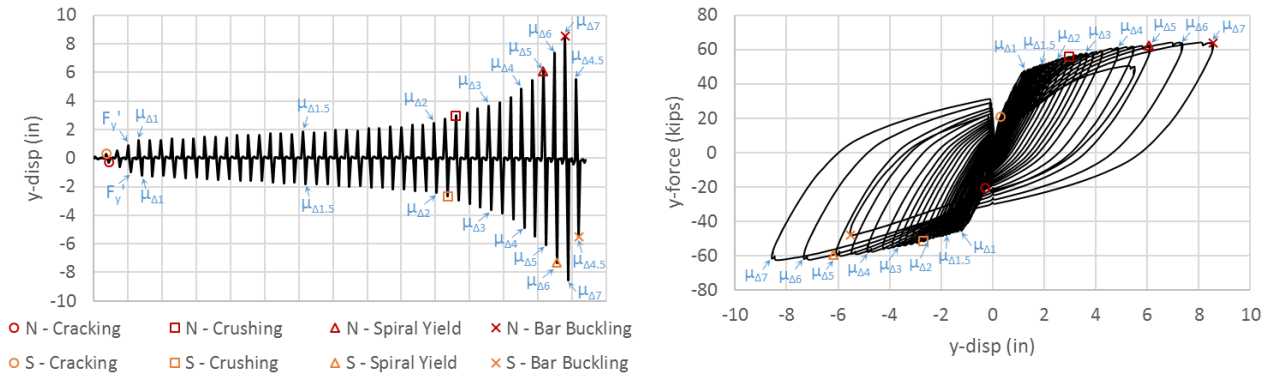


**Fig. 3 – Test #11 Megathrust Load History and Hysteretic Response (Y-direction Loading)**

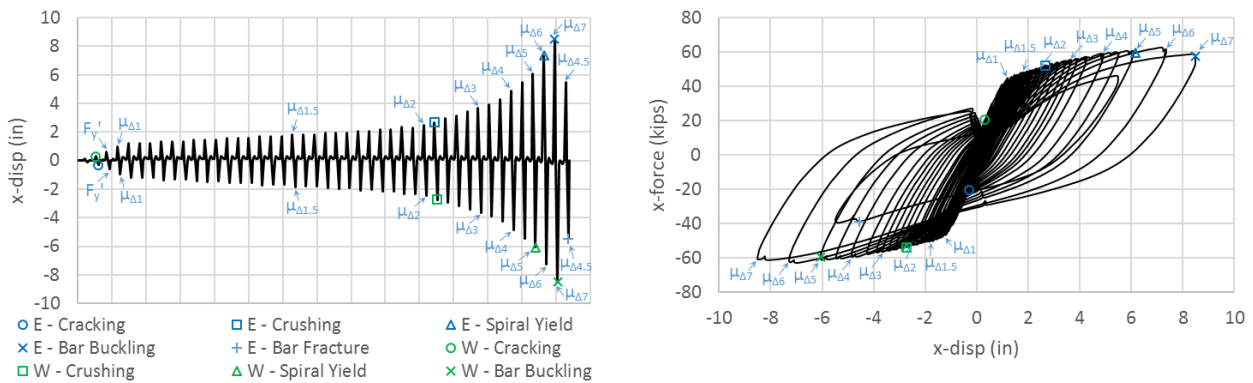


**Fig. 4 – Test #11 Megathrust Load History and Hysteretic Response (X-direction Loading)**

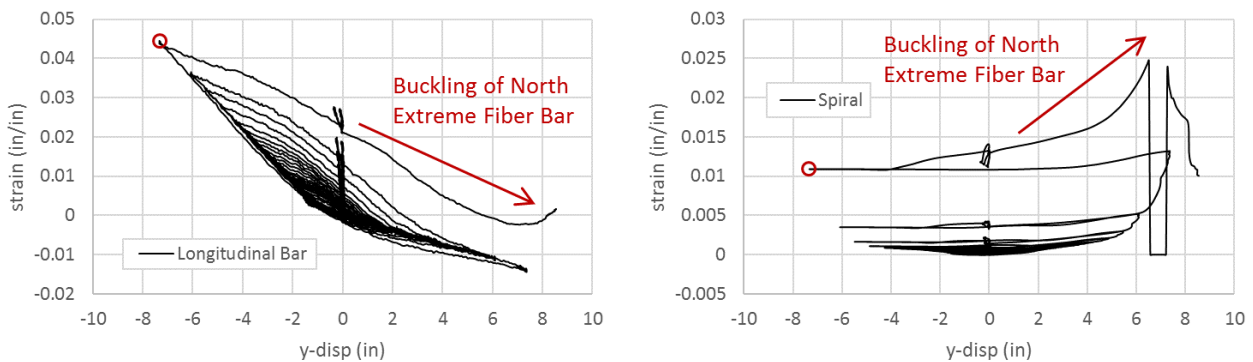


**Fig. 5 – Test #11 Longitudinal Steel and Spiral Restraint Hysteresis in Region of Reinforcement Buckling**

Measured strain data for both the north extreme fiber longitudinal bar and its critical layer of spiral restraint that overlaid the region of outward bar buckling appears in Fig. 5. The north extreme fiber region experienced compression during positive y-direction loading and represents the location of first bar buckling in Test #11. Confinement reinforcement yielded under compressive demands during displacement ductility five, as shown in Fig. 3. Initial yielding of confinement steel led to a decrease in the stiffness of restraint for longitudinal reinforcement, which often led to measurable outward deformation prior to visible observations of bar buckling. A peak tensile strain of 0.044 was measured in the north extreme fiber bar at displacement

ductility six, prior to observed bar buckling during the subsequent peak reversal to displacement ductility seven. Beyond initial bar buckling, repeated cycles buckled adjacent reinforcement and led to increased damage to the core concrete behind the buckled deformation where the confinement steel is no longer effective.

All sixteen longitudinal bars were instrumented to obtain strains at horizontal sections in the plastic hinge region, see Fig. 1. Cross section curvatures were obtained as the slope of a linear regression through the measured strain profile. Curvature profiles were then constructed as shown in Fig. 6. The grey dashed line represents the equivalent yield curvature distribution, which closely matched the measured curvatures at displacement ductility one. Plastic curvatures were found to follow a linear distribution and procedures from [9] were followed to extract important information regarding their shape. A linear regression was fit to the plastic portion of each curvature profile. The base section curvature was obtained as the intersection of the linear regression with the footing-column interface. The extent of plasticity,  $L_{pr}$ , was computed as the intersection of the linear plastic curvature regression and the equivalent yield curvature profile.

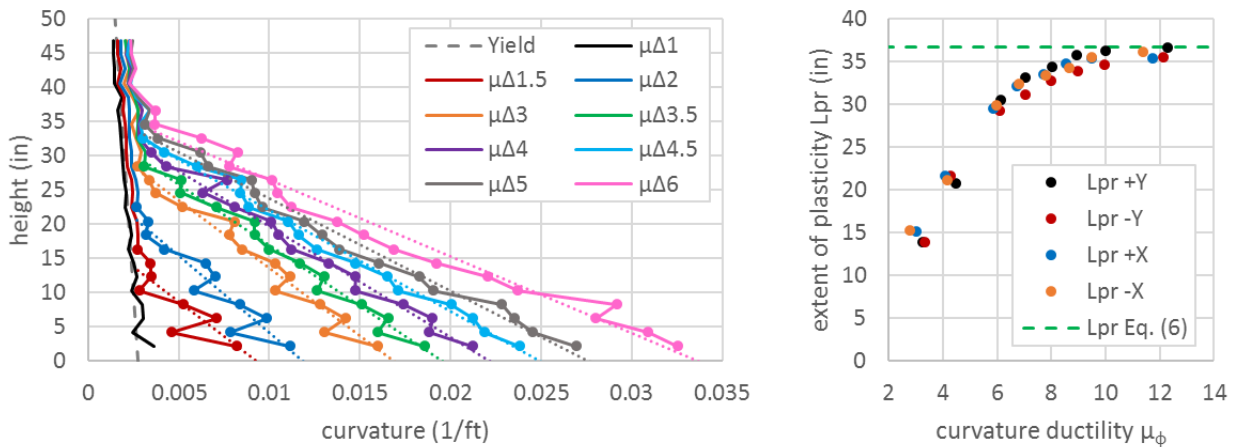


**Fig. 6** – Test #11 Measured Curvature Profiles and Extent of Plasticity Compared to  $L_{pr}$  in Eq. (6)

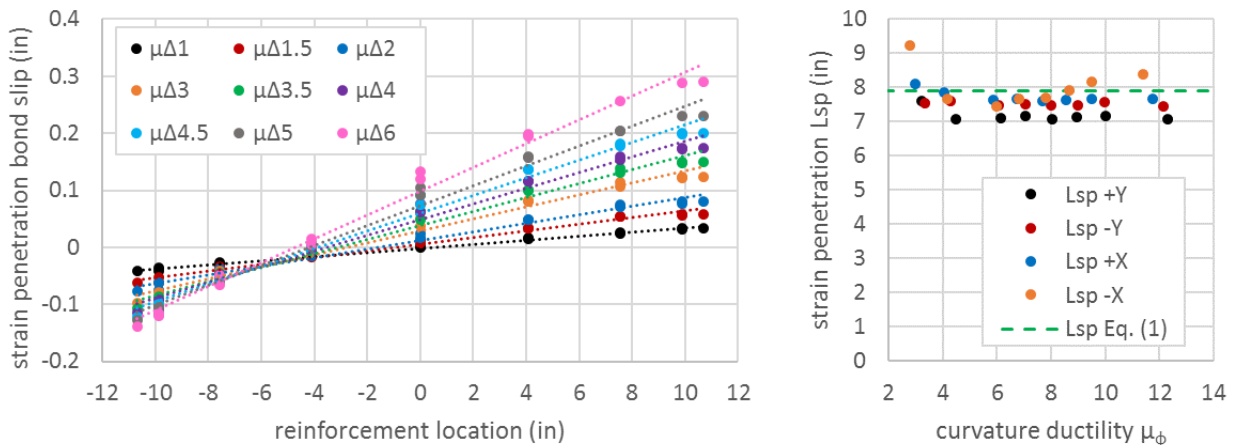


**Fig. 7** – Test #11 Measured Fixed-End Rotation Due to Strain Penetration Compared to  $L_{sp}$  in Eq. (1)

The spread of plasticity in the tests is due to the combined effects of moment gradient and tension shift. The moment gradient effect can be described as the influence of larger base section moments on the distribution of moment and thus curvature along the column length. Compressive strains are concentrated near the footing, while tension strains are fanned out to a greater height following the inclined flexural shear crack distribution. This behavior is known as tension shift. The measured spread in plasticity,  $L_{pr}$ , is plotted in Fig. 6 as a function of base section curvature ductility. The upper bound to the measured spread in plasticity defines the length of the plastic hinge region and is referenced in subsequent discussions regarding plastic hinge lengths.

Development of fully anchored column longitudinal bars into the footing leads to bond slip along the partially anchored region of the bars near the footing-column interface, as described in [10]. This bond slip was computed as the vertical displacement of instruments placed closest to the footing-column interface. Fixed-end rotations attributable to strain penetration of reinforcement into the adjoining member were computed as the slope of a regression through the measured bond-slip profile in Fig. 7. An equivalent strain penetration length is obtained by dividing the fixed-end rotation by the base section curvature, representing the geometry of an equivalent rectangular curvature block centered at the footing-column interface. The computed equivalent strain penetration lengths,  $L_{sp}$ , for Test #11 agree with Eq. (1), which is included in the plastic hinge lengths of [5&6]. In general, computed  $L_{sp}$  values in other tests were often smaller than predicted with Eq. (1), but no changes are recommended as accurate strain-displacement results were still achieved.

## 2. Modifications to the Plastic Hinge Method for Member Deformations

Modifications to the plastic hinge method for member deformations were made using the measured strain, curvature, and fix-end rotations to improve the accuracy of strain-displacement predictions essential for use of strain limits in performance-based seismic design. This paper provides improvements over prior recommendations in [3] by including results from the more recent bidirectional dataset. Bidirectional loading was observed to increase the measured spread of plasticity,  $L_{pr}$ . Additional details can be found in [2].

### 2.1 Compressive and Tensile Plastic Hinge Lengths

The plastic hinge method is used to simplify the real nonlinear plastic curvature distribution into an equivalent simplified rectangular distribution for design. The height of the simplified distribution, see Fig. 8, is termed the plastic hinge length,  $L_p$ , while the width is set to the plastic curvature at the base section. A key component of the modified plastic hinge method is the use of separate compressive and tensile plastic hinge lengths. Both moment gradient and tension shift contribute to the total spread in plasticity,  $L_{pr}$ , measured in the experiments, see Fig. 6. Tensile strains were found to be proportional to this total spread in plasticity,  $L_{pr}$ , while compression strains were found to be more influenced by only the moment gradient component of the spread in plasticity. Note the difference in geometry between the triangular  $L_{pr}$  and rectangular  $L_p$  in Figs. 6 and 8.

The simplified rectangular compressive plastic hinge length in Eq. (3) matches current Seismic Guide Specifications [5&6] recommendations. In Eq. (3),  $kL_c$  represents the moment gradient contribution to the spread in plasticity while  $L_{sp}$  represents the effect of strain penetration of longitudinal reinforcement into the adjoining member. Where  $L_c$  is the length from the critical section to the point of contraflexure and  $d_{bl}$ ,  $f_{ye}$ , and  $f_{ue}$  are the diameter and expected material properties of the longitudinal reinforcement.

Through displacement equivalency evaluated with the moment-area method, it can be shown that the equivalent rectangular plastic hinge length  $L_p$  is half the height of the triangular plastic hinge length  $L_{pr}$ . In its basic form, the triangular tensile plastic hinge length in Eq. (6) was created to match the upper bound spread of plasticity measured in each test, see Fig. 6. In Eq. (6), the term 0.8D represents the additional spread in plasticity due to tension shift in the bidirectional experiments, while a smaller value of 0.66D was appropriate for the unidirectional tests. Table 2 provides a comparison of the upper bound to the measured spread of plasticity and the results of Eq. (6) in respective datasets. Using the noted geometric conversion for equivalency and including the strain penetration component of deformation, the rectangular tensile plastic hinge length in Eq. (4) is obtained. Similarly, a smaller value of 0.33D in Eq. (4) is appropriate for unidirectional response; however, this value is less useful in design where bidirectional demands often govern.

The compressive hinge length is used for both compressive strain-displacement and for predictions of member force versus deformation, thus nonlinear static pushover procedures remain unchanged and the tensile hinge length is exclusively used to convert plastic curvatures at tensile strain limits to lateral displacements.

$$L_{sp} = 0.15f_{ye}d_{bl} \quad \text{Equivalent Strain Penetration Length (ksi units)} \quad (1)$$

$$k = 0.2 \left( \frac{f_{ue}}{f_{ye}} - 1 \right) \leq 0.08 \quad \text{Moment Gradient Coefficient} \quad (2)$$

$$L_{pc} = kL_c + L_{sp} \geq 2L_{sp} \quad \text{Compressive Plastic Hinge Length} \quad (3)$$

$$L_{pt} = L_{pc} + 0.4D \quad \text{Tensile Plastic Hinge Length (Bidirectional)} \quad (4)$$

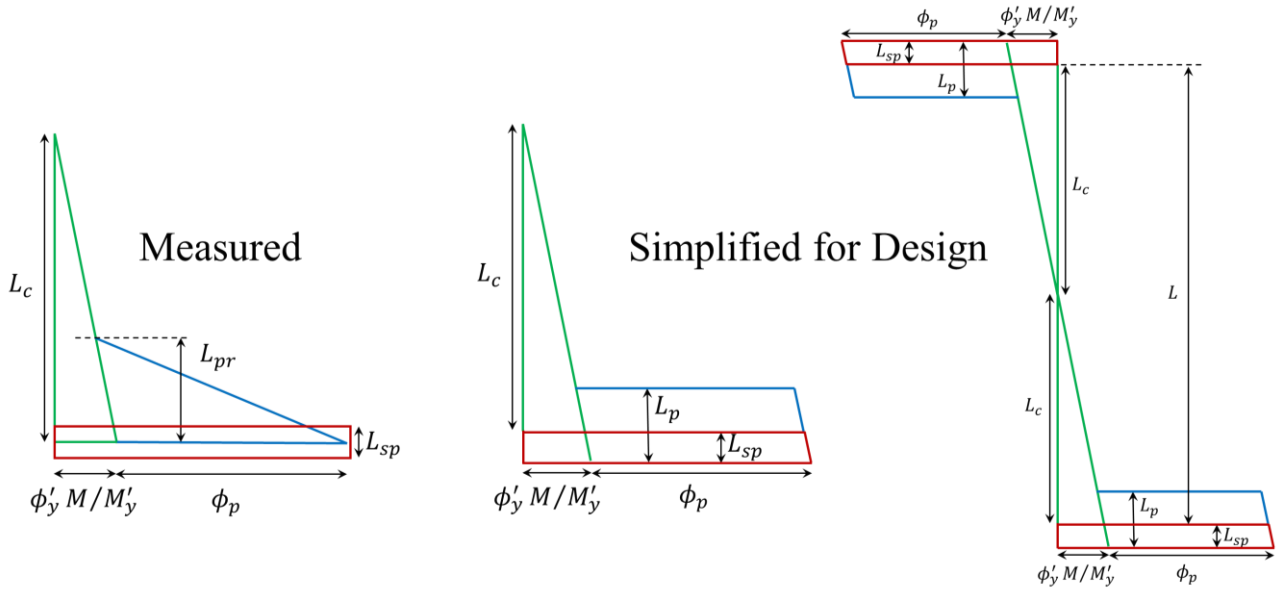


**Fig. 8** – Equivalent Curvature Distributions for Columns in Single and Double Bending

$$L_{prc} = 2kL_c \geq 2L_{sp} \quad \text{Triangular Compressive Plastic Hinge Region} \quad (5)$$

$$L_{prt} = L_{prc} + 0.8D \quad \text{Triangular Tensile Plastic Hinge Region (Bidirectional)} \quad (6)$$

**Table 2** – Comparison of Measured and Predicted Extent of Plastic Hinge Region,  $L_{pr}$

Column Dataset	Mean Measured Extent of Plasticity / $L_{prt}$ in Eq. (6)	COV
Unidirectional (0.66D)	1.002	0.072
Bidirectional (0.8D)	1.000	0.026
Combined	1.002	0.060

## 2.2 Simplified Equivalent Curvature Distributions for Design

Simplified equivalent curvature distributions provide a means to compute column flexural displacements that aid in checking the results for nonlinear static pushover and nonlinear response history analyses. The equations reflect application of the moment-area method to the simplified geometry in Fig. 8. A similar set of equations for the more realistic triangular plastic curvature distribution that decouples column flexural and strain-penetration displacements can be found in [2]. In Fig. 8,  $M'_y$  and  $\phi'_y$  are the moment at curvature at first yield.

### 2.2.1 Flexural Displacements for a Member in Single Bending (Fixed-Free)

The following equations are used to compute the flexural displacement of a column in single bending.

$$\Delta_e = \phi_{base} (L + L_{sp})^2 / 3 \quad \text{(Single) Elastic Displacement Prior to First-Yield} \quad (7)$$

$$\Delta_e = \phi'_y (M/M'_y) (L + L_{sp})^2 / 3 \quad \text{(Single) Elastic Displacement Beyond First-Yield} \quad (8)$$

$$\phi_p = \phi_{base} - \phi'_y(M/M'_y) \quad \text{(Single) Plastic Curvature at the Base Section} \quad (9)$$

$$\Delta_p = \phi_p L_p (L + L_{sp} - 0.5L_p) \quad \text{(Single) Plastic Flexural Displacement} \quad (10)$$

$$\Delta_f = (\Delta_e + \Delta_p) \quad \text{(Single) Total Column Flexural Displacement} \quad (11)$$

### 2.2.2 Flexural Displacements for a Member in Double Bending (Fixed-Fixed)

The following equations are used to compute the flexural displacement of a column in double bending.

$$\Delta_e = \phi_{base} (L + 2L_{sp})^2 / 6 \quad \text{(Double) Elastic Displacement Prior to First-Yield} \quad (12)$$

$$\Delta_e = \phi'_y (M/M'_y) (L + 2L_{sp})^2 / 6 \quad \text{(Double) Elastic Displacement Beyond First-Yield} \quad (13)$$

$$\phi_p = \phi_{base} - \phi'_y (M/M'_y) \quad \text{(Double) Plastic Curvature at the Base Section} \quad (14)$$

$$\Delta_p = \phi_p L_p (L + 2L_{sp} - L_p) \quad \text{(Double) Plastic Flexural Displacement} \quad (15)$$

$$\Delta_f = (\Delta_e + \Delta_p) \quad \text{(Double) Total Column Flexural Displacement} \quad (16)$$

### 2.3 Modified Plastic Hinge Method Comparison to Measured Response

A comparison of the accuracy of strain-displacement predictions at key performance limit states using either the modified plastic hinge method or the Seismic Guide Specification [5&6] approach appears in Table 3. Again, there is no change in the compressive plastic hinge length of Eq. (3), but the slight differences in compressive strain-displacement in Table 3 arise only due to the use of the triangular compressive plastic hinge length in Eq. (5) and the decoupled strain-penetration curvature block shown in Fig. 8. As the results of Table 3 would imply, the differences in compressive strain-displacement are minor and design simplifications based on a rectangular plastic hinge length are appropriate. Use of the tensile plastic hinge length in the modified approach significantly increases the accuracy of tensile strain-displacement predictions at bar buckling.

**Table 3** – Measured and Predicted Displacement at Key Limit States in the Combined Dataset

Measured Occurrence of Limit State	Model	Mean Measured / Predicted Disp.	COV
Analytical First Yield Force Fy'	Guide Spec	1.145	0.087
	Modified	1.079	0.084
Cover Concrete Crushing Strain	Guide Spec	0.858	0.193
	Modified	1.017	0.177
Initial Confinement Steel Yielding Strain	Guide Spec	0.799	0.255
	Modified	0.805	0.252
Longitudinal Bar Buckling Strain	Guide Spec	1.291	0.091
	Modified	0.989	0.072

## 3. Material Strain Limits for Performance-Based Seismic Design

### 3.1 Serviceability Strain Limits

When exceeded, serviceability limit states represent the point at which repair becomes necessary, interrupting the serviceability of the structure, but not posing a safety concern. The serviceability limit states are characterized by initial crushing of cover concrete and residual crack widths that exceed 1 mm, which require some degree of intervention to prevent corrosion of internal reinforcing steel. No changes are recommended

to the serviceability strain limits proposed in [7&11], which are repeated in Eq. (17) and Eq. (18). The serviceability strain limits are consistent with the essentially elastic performance objective in a lower level earthquake that allows for limited hinge formation, but damage consistent with immediate occupancy.

The average measured compressive strain at cover concrete crushing was 0.005, although observations were made at the cycle peaks with larger strains. Crushing observations were rather crude due to the partial removal of cover concrete, where instead initial crushing was defined as the first visual flaking of concrete between spiral layers. Under the magnitude of imposed compression, these regions are influenced less by the passive confinement provided by the spiral reinforcement. A comparison of measured displacements at initial cover crushing and those evaluated with Eq. (17) and the modified plastic hinge method appears in Table 4. For the subject experiments, initial crushing governed over the threshold residual crack width expression.

$$\varepsilon_c = 0.004 \quad \text{Cover Concrete Compression Strain at Initial Crushing} \quad (17)$$

$$\varepsilon_s = 0.015 \quad \text{Extreme Steel Tensile Strain Related to 1mm Residual Crack Widths} \quad (18)$$

**Table 4** – Cover Concrete Crushing Displacement Predictions using the Modified Plastic Hinge Method

Limit State	Dataset	Measured / Predicted Displacement	
		Mean	COV
Cover Crushing $\varepsilon_c = 0.004$	Bidirectional	1.249	0.132
	Unidirectional	0.902	0.143
	Combined	1.087	0.210

### 3.2 Damage Control Strain Limits

The damage control limit state represents the limit of economical repair, and is defined by longitudinal bar buckling or significant damage to the core concrete. The damage control limit states are consistent with life safety performance criteria applied in the Seismic Guide Specifications [5] to the design (upper level) earthquake. Bar buckling was observed to occur after reversal from a peak tensile strain while the bar was under net elongation, but compressive stress. Although prior compression was important for describing the stiffness of restraint provided by the transverse steel, expressions developed based on peak tensile strains were found to produce the most accurate results. Furthermore, higher levels of tensile strain reduce the tangent modulus of the reinforcement during the subsequent stress reversal, influencing the inelastic buckling behavior. Instrumentation placed on the longitudinal bars and spiral restraint indicated that outward measurable deformation often occurred prior to visible bar buckling observations.

Using the measured reinforcement strains, an expression for the peak tensile strain preceding bar buckling was developed in Eq. (19). In the expression,  $\rho_s = 4A_{sp}/D's$  is the transverse volumetric steel ratio,  $f_{yhe}/E_s$  is the yield strain of the transverse reinforcement, and  $P/f'_{ce}A_g$  is the axial load ratio under dead loads. Modification to the axial force for seismic overturning effects is unwarranted due to the current lack of experimental data to validate the approach. Sufficient confinement steel should be provided such that the Mander [12] ultimate concrete compressive strain in Eq. (20) exceeds core concrete strains at the bar buckling displacement, otherwise Eq. (20) governs the damage control limit state. Expected material properties should be used in both expressions. Although Eq. (20) was derived based on energy balance between core concrete dilation under uniform axial compression and the confining steel at hoop fracture, flexural column tests indicate that Eq. (20) is consistently conservative [7&11], and instead correlates to levels of core concrete damage that begins to influence buckling of longitudinal reinforcement. Hoop fracture was observed only once in the subject experiments, and was attributed to increased buckled deformation under bidirectional demands.

$$\varepsilon_{sbb} = 0.032 + 790\rho_s \frac{f_{yhe}}{E_s} - 0.14 \frac{P}{f'_{ce}A_g} \quad \text{Peak Tensile Strain Prior to Bar Buckling} \quad (19)$$

$$\epsilon_{c_u} = 0.004 + \frac{1.4\rho_s f_{yhe}\epsilon_{uh}}{f'_{cce}} \quad \text{Mander [12] Ultimate Concrete Compression Strain} \quad (20)$$

A comparison of measured peak tension strains and displacements preceding bar buckling and those evaluated with Eq. (19) and the modified plastic hinge method appears in Table 5. Cumulative probability distributions plot the variability in the bar buckling strain and displacement predictions in Fig. 9. A similar comparison using the Mander [12] ultimate concrete compression strain in Eq. (20) appears in Table 6.

**Table 5** – Bar Buckling Displacement Predictions using the Modified Plastic Hinge Method

Limit State	Dataset	M/P Strain		M/P Displacement	
		Mean	COV	Mean	COV
Bar Buckling $\epsilon_{S_{bb}}$ in Eq. (19)	Bidirectional	1.006	0.119	0.993	0.111
	Unidirectional	1.006	0.167	1.012	0.187
	Combined	1.006	0.143	1.002	0.153

**Table 6** – Bar Buckling Displacement Predictions using the Modified Plastic Hinge Method

Limit State	Dataset	M/P Peak Displacement Preceding Bar Buckling	
		Mean	COV
Mander [12] Ultimate Comp. $\epsilon_{c_u}$ in Eq. (20)	Bidirectional	0.993	0.140
	Unidirectional	0.936	0.189
	Combined	0.965	0.166

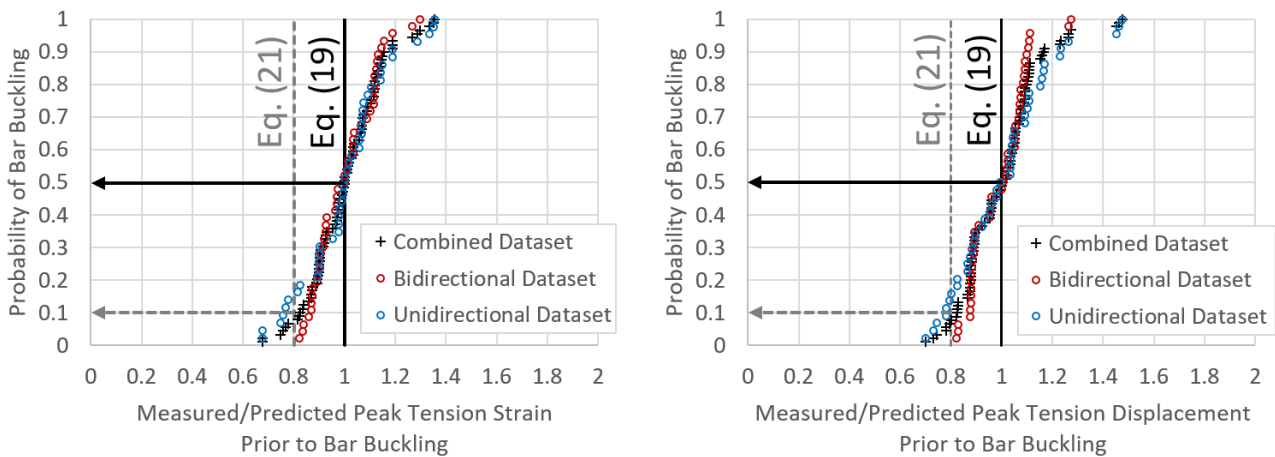


**Fig. 9** – Cumulative Probability Distributions for Measured/Predicted Strain and Disp. Prior to Bar Buckling

### 3.2.1 Bar Buckling Predictions for an Independent Bridge Column Dataset

Bar buckling predictions using Eq. (19) and the modified plastic hinge method were made for thirty-six bridge columns with reported bar buckling observations in the literature compiled into a dataset in [13]. Additional details regarding specific columns included in the evaluation can be found in [2]. Results appear in Fig. 10 in the form of a cumulative probability distribution. For bridge columns in the independent dataset, a mean measured-to-predicted bar buckling displacement ratio of 1.191 was computed with a coefficient of variation (COV) of 0.324 when using Eq. (19) and the modified plastic hinge method.

### 3.3 Tensile Strain Limit Related to Reduced Probability of Bar Buckling

For bridges with need for a higher standard of performance in the design earthquake, a tensile strain related to a reduced probability of initial bar buckling was created in Eq. (21) using the results of the cumulative probability distributions in Figs. 9 and 10. Note that Eq. (21) simply represents 80% of the result of Eq. (19) and corresponds roughly to a 10% probability of bar buckling in each dataset.

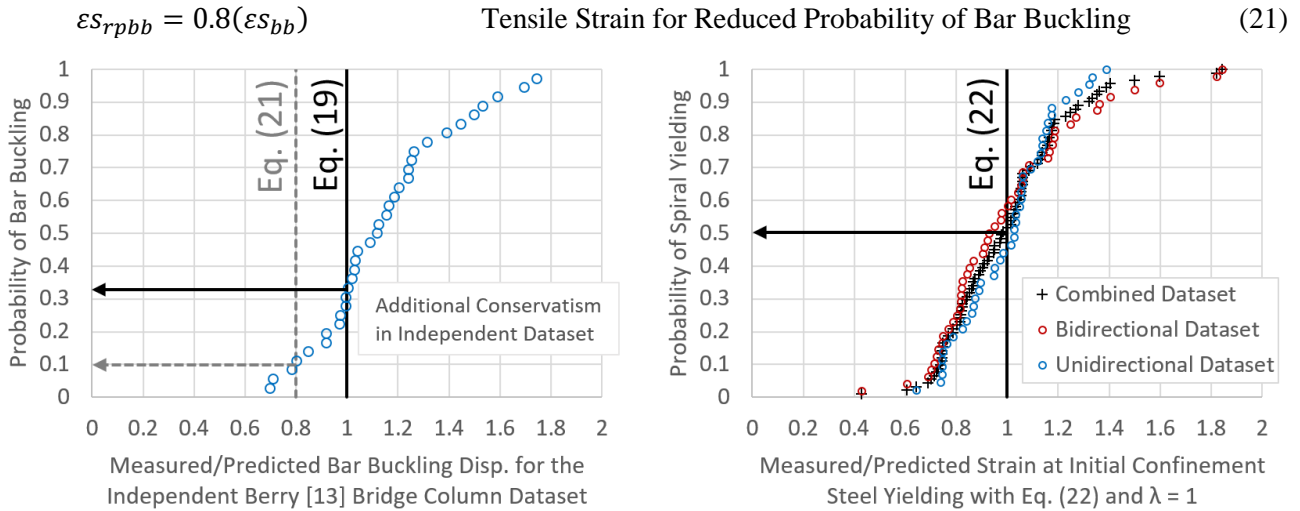


**Fig. 10** – (Left) Cumulative Probability Distributions for Bar Buckling in the Berry (2006) Dataset [13] and (Right) Cumulative Probability Distributions for Measured/Predicted Comp. Strain at Initial Spiral Yield

### 3.4 Intermediate Compressive Strain Limit Prompting a Change in Repair Strategy

Yielding of confinement steel under compressive demands occurred prior to longitudinal bar buckling in each experiment. Inelastic transverse steel offers a reduced restraint stiffness that often allowed for measureable outward deformation of longitudinal reinforcement prior to visible bar buckling observations. As a limit state, yielding of confinement steel prompts a change in repair strategy from epoxy injection of cracks and patching of cover concrete, to the need for additional transverse stiffness via either FRP wraps or steel jackets within the plastic hinge region. In extreme fiber regions, transverse steel is subjected to both confinement demands and those associated with restraint of longitudinal reinforcement. Columns with higher longitudinal steel ratios required additional restraint, which decreased the remaining strain component for confinement, thus reducing core concrete compressive strains at initial yielding of transverse reinforcement.

An expression that predicts the core concrete compressive strain at initial yielding of confinement steel appears in Eq. (22). In the expression,  $A_{st}/A_g$  is the longitudinal steel ratio and  $\lambda$  is a compression strain-displacement modification factor. In Eq. (22), setting  $\lambda = 1$  provides strains that match measured values, while selecting  $\lambda = 0.8$  compensates for the unconservative compressive strain-displacement predictions when using the compressive plastic hinge in Eq. (3), see Table 3. A comparison of measured core concrete compression strains and displacements at initial yielding of confinement steel and those evaluated with Eq. (22) and the modified plastic hinge method appears in Table 7. A graphical comparison of strains is shown in Fig. 10.

$$\varepsilon_{c_{sy}} = \lambda \left( 0.022 - 0.48 \frac{A_{st}}{A_g} \right) \quad \text{Core Concrete Strain at Initial Confinement Steel Yield} \quad (22)$$

**Table 7** – Initial Yielding of Confinement Steel Predictions using the Modified Plastic Hinge Method

Limit State	Dataset	M/P Strain ( $\lambda = 1$ )		M/P Disp. ( $\lambda = 0.8$ )	
		Mean	COV	Mean	COV
Initial Spiral Yielding $\varepsilon_{c_{sy}}$ in Eq. (22)	Bidirectional	1.005	0.295	1.015	0.133
	Unidirectional	1.001	0.182	0.870	0.239
	Combined	1.003	0.247	0.945	0.198

### 3.5 Limits of Applicability of the Performance Strain Limit Expressions

The limits of applicability of Eqs. (19, 21, and 22) can be stated as follows:  $P/f'_{ce}A_g \leq 0.30$ ,  $\rho_s f_{yhe}/f'_{ce} \geq 0.05$ ,  $A_{st}/A_g \leq 0.04$ ,  $s/d_{bl} \leq 6$ , and  $cover/D \leq 0.1$ . The limits reflect the datasets used in the comparison.

## 4. Conclusions

This paper discussed performance strain limit and plastic hinge length recommendations for displacement-based seismic design of circular reinforced concrete bridge columns. These recommendations were obtained via analysis of results from thirty unidirectional [1] and twelve bidirectional [2] experiments that contained instrumentation capable of measuring distributions of strain and curvature along the member length. The main experimental variables included longitudinal and transverse steel content, axial load ratio, aspect ratio, and lateral displacement history. Expressions that predict concrete and steel strains preceding important limit states were created, which included: cover concrete crushing, initial yielding of confinement steel, and longitudinal bar buckling. Since bar buckling, and subsequent fracture, limited the deformation capacity of the well-confined columns, separate expressions that provided either a mean value prediction or a reduced probability of bar buckling were produced. A modified plastic hinge method was created to convert curvatures at limit state strains to lateral displacements. Separate tensile and compressive plastic hinge lengths were recommended for respective conversions of material strain to displacement. The tensile plastic hinge length was formulated to match the measured extent of plasticity, which also provided accurate tensile strain-displacement relationships necessary for bar buckling predictions. The compressive plastic hinge length matches current AASHTO Guide Specifications for LRFD Seismic Bridge Design [5] recommendations, which reference the approach in [6]. The compressive plastic hinge length is used for both compressive strain-displacement and for predictions of member force versus deformation, thus nonlinear static pushover procedures remain unchanged and the tensile hinge length is exclusively used to convert plastic curvatures at tensile strain limits to lateral displacements. Thus, a separate nonlinear static pushover is not required.

## 5. References

- [1] Goodnight JC, Kowalsky MJ, Nau JM (2015): The Effects of Load History and Design Variables on Performance Limit States of Circular Bridge Columns. *Report No. 4000(72) Volumes 1 and 2*, AKDOT&PF, Juneau, Alaska.
- [2] Goodnight JC, Kowalsky MJ, Nau JM (2017): Seismic Load Path Effects in Reinforced Concrete Bridge Columns and Wall Piers. *Report No. 4000(134) Volume 1*, AKDOT&PF, Juneau, Alaska.
- [3] Goodnight JC, Kowalsky MJ, Nau JM (2016): Modified Plastic Hinge Method for Circular RC Bridge Columns. *Journal of Structural Engineering*, **142** (11), (doi: 10.1061/(ASCE)ST.1943-541X.0001570).
- [4] Goodnight JC, Kowalsky MJ, Nau JM (2016): Strain Limit States for Circular RC Bridge Columns. *Earthquake Spectra*, **32** (3), 1627-1652.
- [5] AASHTO Guide Specifications for LRFD Seismic Bridge Design 2nd Edition (2011 with 2015 Interim Revisions)
- [6] Priestley MJN, Seible F, Calvi GM (1996): *Seismic Design and Retrofit of Bridges*. John Wiley & Sons, New York.
- [7] Priestley MJN, Calvi GM, Kowalsky MJ (2007): *Displacement-Based Seismic Design of Structures*, IUSS Press, Pavia, Italy.
- [8] Bazaez R, Dusicka P (2016): Cyclic Loading for RC Bridge Columns Considering Subduction Megathrust Earthquakes. *Journal of Bridge Engineering*, **21** (5), (doi:10.1061/(ASCE)BE.1343-5592.0000891).
- [9] Hines EM, Seible F (2002): *Experimental Spread of Plasticity in Reinforced Concrete Bridge Piers*. *Structural Systems Research Project 2001/08*, San Diego, La Jolla, California: University of California.
- [10] Zhao J, Sritharan S (2007): Modeling of Strain Penetration Effects in Fiber-Based Analysis of Reinforced Concrete Structures. *ACI Structural Journal*, **104** (2), 133-141.
- [11] Kowalsky MJ (2000): Deformation Limit States for Circular Reinforced Concrete Bridge Columns. *Journal of Structural Engineering*, **126** (8), 869-878.
- [12] Mander JB, Priestley MJN, Park R (1988): Theoretical Stress-Strain Model for Confined Concrete. *Journal of Structural Engineering*, **144** (8), 1804-1826.
- [13] Berry MP (2006). *Performance Modeling Strategies for Modern Reinforced Concrete Bridge Columns*. PhD Thesis, Seattle, Washington: University of Washington.